# **Bioinspiration & Biomimetics**



RECEIVED

27 June 2018

REVISED 29 October 2018

ACCEPTED FOR PUBLICATION 18 December 2018

PUBLISHED 23 January 2019

# NOTE

# Robotic device shows lack of momentum enhancement for gymnotiform swimmers

Ian English, Hanlin Liu and Oscar M Curet®

Department of Ocean and Mechanical Engineering, Florida Atlantic University, Boca Raton, FL, 33431, United States of America E-mail: ocuret@fau.edu

Keywords: fish swimming, undulatory fin propulsion, momentum enhancement, underwater robot, bio-fluid dynamics

#### **Abstract**

Many fish generate thrust by undulating one or multiple elongated fins while keeping their body straight. This propulsion mechanism has stimulated interest in both biology and bio-inspired marine propulsion because its maneuverability and efficiency at low speed. Analytical studies have found that a fin attached to a rigid flat body can produce substantially higher thrust compared to a fin without a body, three- to four-fold for natural swimmers. However, this momentum enhancement has not been confirmed experimentally. In this work, a robotic ribbon fin model with an adjustable-height body was used to test the momentum enhancement for gymontiform swimmers where the undulating fin runs along the ventral side of the body. In a series of experiments, the force generated by the robotic device was measured as the body height of the robot, the undulating fin frequency and the flow speed were changed. It was found that the thrust generated by the ribbon fin is not affected by the presence of a body, thereby resulting in no momentum enhancement due to the fin-body interaction. These results suggest that if there is a benefit at a specific fin-body height ratio of the fishes, the momentum enhancement is not the reason. This result has broader implications in understanding the evolutionary adaption of undulatory fin propulsion and underwater vehicles designs.

# Introduction

Although most ray-finned fishes use their bodies or pectoral fins as primary propulsion mechanism, there are numerous fishes propelled by undulating a thin low aspect ratio membrane. This elongated fin is composed of many flexible bonny-rays interconnected by an elastic membrane. The location of the undulating fin can be found in the dorsal side, ventral side or both dorsal and ventral sides of the fish. This propulsion method is of particular interest because it is highly efficient at low speeds [1], and it is use as a model for highly maneuverable underwater vehicles [2, 3, 20]. Depending on the location of the fin(s), the swimming style is classified as gymnotiform (ventral fin), amiiform (dorsal fin) or ballistiform (dorsal and ventral fins). In series of studie Lighthill and Blake [4] and Lighthill [5-7] investigated the thrust generation of an undulating fin attached to rigid body. Based on a theoretical model, they found that an undulating fin with a body was able to generate more thrust than an undulating fin without body, referring to this effect as momentum enhancement. This momentum enhancement could be as much as three to four times for the fin-body aspect ratio found in nature. This effect has broader implications to understand the convergent evolution of the body-fin design found in this type of swimming mechanism. Moreover, it could guide the design and development of underwater vessels using undulating fins for propulsion and maneuver controls [2, 20]. Unfortunately, there has been not direct experimental work validating these results.

Ribbon-fin based propulsion has independently evolved multiple times during geological periods and in very different environments including deepsea (oarfish), shallow waters in coral reefs (seahorses and triggerfish) as well as rivers and lakes (e.g. knifefishes, bowfin, mooneyes) [8, 9], as seen in figure 1. The convergent evolution of this type of propulsion mechanism also spans a wide range of length that scales from a few centimeters (glass knifefish) to tens of meters (giant oarfish, *Regalecus glesne*). It has been suggested that this propulsion mechanism is an evolutionary adaption to swim with high efficiency at low speeds [10] and that this swimming mode exhibits

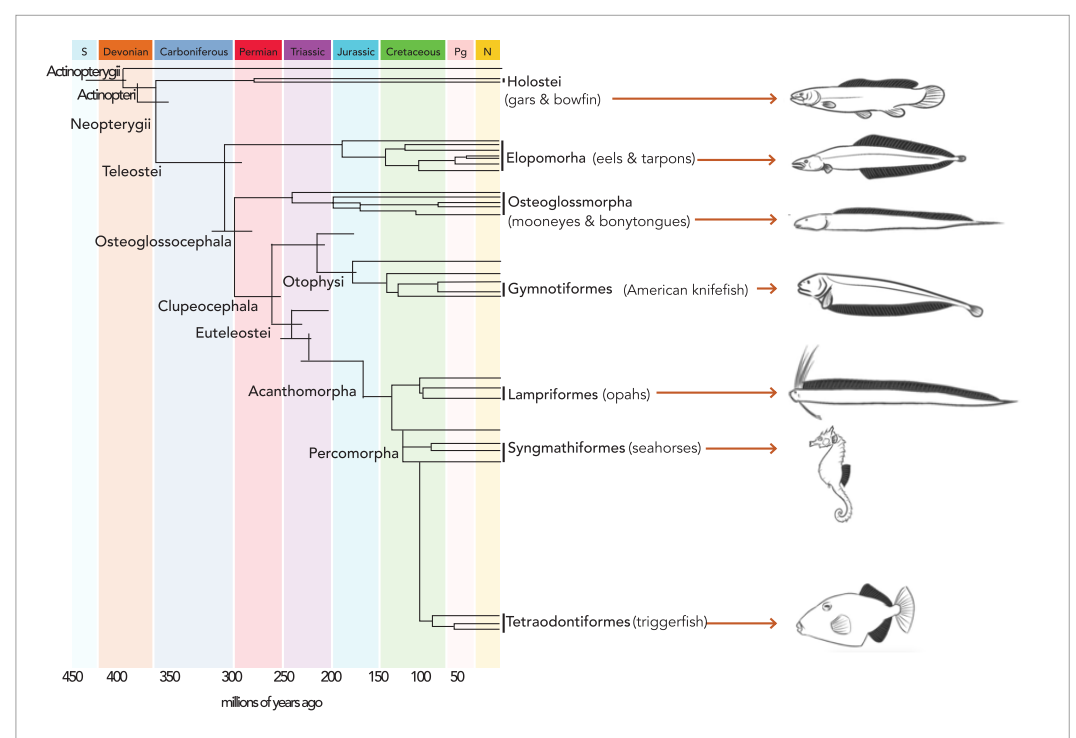


Figure 1. Representative fishes of undulating ribbon-fin based propulsion in context to ray-finned phylogeny and time of diversification. These fishes undulate an elongated dorsal and/or ventral fin (shown in dark) to swim. This type of propulsion has evolved multiple times at different geological periods for both fresh and seawater. Fish schematics are not shown to scale. Adapted with permission from [9] and [8] John Wiley & Sons. © 2013 Wiley Periodicals, Inc.

a convergent evolution of optimal mechanical locomotion [11]. In addition, this swimming mode can lead to impressive locomotor capabilities as observed in the maneuvers of knifefishes [12].

Lighthill and Blake pioneered the research of ribbon-fin based locomotion with a wide range of studies for electric eels, knifefish, and triggerfish. In 1971, Lighthill developed the elongated-body theory of fish locomotion. Blake [10] studied the locomotion of gymnotiform swimmers and reported that the drag coefficient of electric eels and knifefishes exceed the theoretical rigid body values. In that work, Blake suggested that the presence of an almost rigid body on top (or bottom) of the undulating fin could provide an additional added mass to the fin (i.e. reaction force to accelerate the fluid around the fin) compared to an isolated fin. Following those studies, Lighthill and Blake [4, 6] investigated the question of whether there is a propulsive advantage of a swimmer with an undulating fin and a rigid body (e.g. gymnotiform, balistiform and amiiform swimmers). They theoretically showed that the thrust generated by an undulatory ribbon fin is enhanced by the presence of a rigid body. This increment was defined using a momentum enhancement factor,  $\beta$ , that is the ratio of the momentum generated by the fin with a rigid body to the momentum of a fin on it's own (2). Since the proposal of this theory, there has been limited research on hydrodynamic interaction between an undulating fin and the body attached to it. Blake and Chan [13] examined the biomechanics and fluid dynamics of puffer-

fish (Diodon holocanthus). Based on computed forces from particle image velocimetry, they argued that the momentum enhancement proposed by Lighthill and Blake is verified. However, real fish experiments are extremely challenging or arguably inadequate to provide a direct proof for momentum enhancement because thrust measurement with and without body cannot be obtained and neither the body or fin height can be systematically changed. Also, the estimation of forces from a planar flow measurement has some clear limitations as the flow are highly three dimensional. Numerical simulations [14, 15] mimicking ribbon fin propulsion found no momentum enhancement. To experimentally examine the momentum enhancement in gymnotiform swimmers a robotic undulating fin model with an adjustable-height body was developed and tested.

Figure 2(A) depicts the momentum enhancement factor found by Lighthill and Blake [4], as a function of the ratio between the body height s, and the height of the body plus the fin l. Although the nature of this type of propulsion is highly three dimensional, they considered a 2D swimmer composed of a thin plate and an oscillating fin. The s/l ratio for most fishes using this propulsion mechanism lies in the range from 0.6 to 0.8, giving a significant momentum enhancement factor between three to four. Lighthill and Blake acknowledged some clear flaws in their results: (1) as s/l tends to zero (i.e. no body but fin), the momentum enhancement does not approach one, and (2) as s/l tends to infinity (i.e. very large body compared to the fin),  $\beta$ 

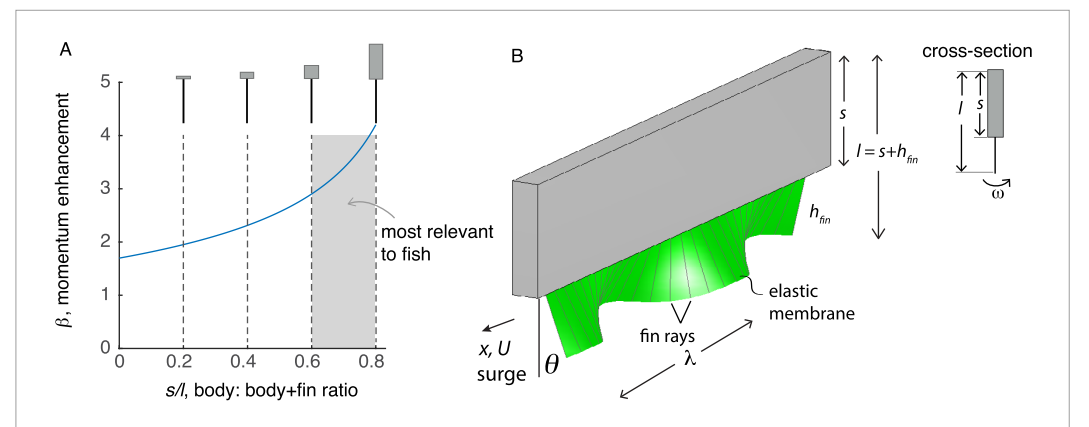
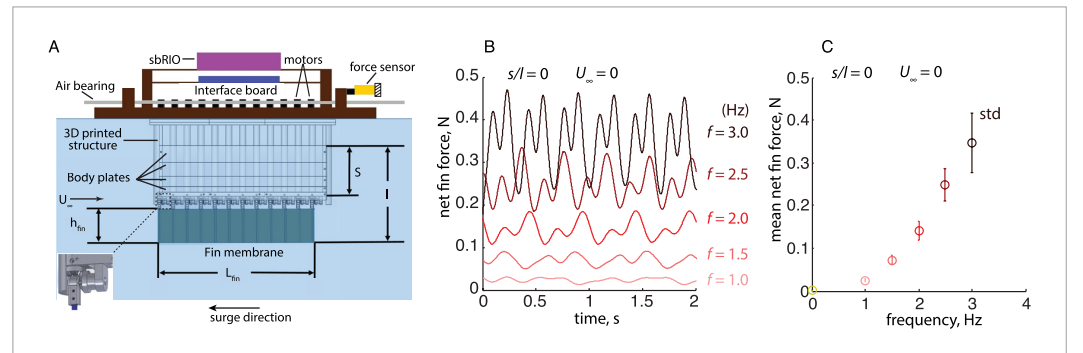


Figure 2. Momentum enhancement. (A) Momentum enhancement factor  $\beta$  as a function of the ratio of body height to the height of body plus the fin (s/l) derived by Lighthill and Blake [4]. The shaded gray area on the graph shows the s/l ratio that is relevant to most fishes using this propulsion mechanism. In this region, the momentum enhancement factor can reach approximately 3–4 compared to a fin with no body. (B) Schematic of the swimmer under consideration: a rigid straight body with an undulating fin of constant height. The fin is composed of multiple rays interconnected with an elastic membrane. The main variables of the fin kinematics includes,  $\theta = \text{fin}$  deflection,  $\lambda = \text{wavelength}$ , angular frequency  $\omega = 2\pi f$ , where f is frequency. x-axis is along the longitudinal axis in the direction of swimming aligned with the surge direction. Inset shows the cross-section of the body with the s, l and angular frequency  $\omega$ .



**Figure 3.** Schematic of the robotic fin with adjustable body and the experimental setup to measure surge force. (A) Experimental setup. The robotic ribbon fin was suspended from a low-friction air bearing system that allowed precise force measurements along the x-axis. The fin was driven by 12 motors, one to control each ray. Different plexiglass panels were used to change the height of the body, s. A 1D load-cell was used to measure the resultant force along the longitudinal axis of the recirculating flume. The robot was tested for incoming flow speeds  $U_{\infty}=0$  and  $11~{\rm cm~s^{-1}}$ . The controller sbRIO, motors and interface board were mounted on the air bearing above the water level. (B) Net force generated by the fin in the surge direction versus time for different undulating frequencies with s/l=0 and  $U_{\infty}=0$ . (C) Mean net force generated by the fin,  $F_{net~fim}$ , as a function of undulating frequency for s/l=0 and  $U_{\infty}=0$ . Vertical lines show the standard deviations of the force.

goes to infinity. For these reasons it is important that the theory is tested experimentally.

To measure the momentum enhancement, a thin-body swimmer was considered with the body height s, that can be varied, and a fin with constant height,  $h_{fin}$ . The key parameters of the fin kinematics are given by the fin angular deflection  $\theta$ , wavelength  $\lambda$  and angular frequency  $\omega = 2\pi f$  where f is the frequency (figure 2(B)). The x-axis is along the longitudinal direction of the fin.

# Material and methods

# Experimental apparatus

Testing momentum enhancement experimentally is challenging due to the requirement of power transmission with 'no-body'. As a compromise, we developed a robotic fin model with long shrouds that

housed the shafts for power transmission to the rays. A schematic of the robotic fin model and experimental setup is depicted in figure 3(A). The robotic device consists of a lower carriage with a wet-section and an upper carriage with the electronic components. The wet section includes a 3D-printed structure, five body plates of different heights and twelve fin rays (Delrin actural resin) interconnected with an elastic Lycra membrane of 23 cm long ( $L_{fin} = 23$  cm) and 5 cm high  $(h_{fin} = 5 \text{ cm})$ . The selection of the material fin rays and fin aspect ratio was based on previous experimental work [16]. The spacing distance between two proximal rays is 2.1 cm. For the kinematics, a sinusoidal traveling wave was considered with a wavelength equal to the fin length ( $\lambda = 23$  cm) and the maximum angular deflection was 20°. Each ray of the fin (twelve in total) were actuated using a maxon motor (RE10, Maxon Motor AG, Sachsein, Switzerland). Each motor had

Table 1. Changing variables for the experiments.

Exp. set	s/l	f (Hz)	$U_{\infty}~({ m cm~s^{-1}})$
1	0	0, 1, 1.5, 2, 2.5, 3	0, 11
2	0.15	0, 1, 1.5, 2, 2.5, 3	0, 11
3	0.32	0, 1, 1.5, 2, 2.5, 3	0, 11
4	0.47	0, 1, 1.5, 2, 2.5, 3	0, 11
5	0.58	0, 1, 1.5, 2, 2.5, 3	0, 11

a 64:1 gear reducer and a 2-channel encoder with 16 counts per revolution. The motors were controlled using a Single-Board Rio (National Instruments). We used a drive shaft enclosed in a shroud to transmit the power from the motor to the rays. The 9-mm-diameter shrouds were 3D printed to provide structural support for the body and fin and avoid the unwanted fluid motion from the shaft rotation. 90-degree bevel gears were used to re-direct the rotational motion of the shafts in the correct orientation, as illustrated in the inset of figure 3(A).

#### **Experimental setup**

Experiments were conducted in a closed-loop circulating water flume with a test section of 0.25 m wide, 0.25 m deep, and 2 m long. The water level in the tests was kept at 0.24 m. The robotic model was mounted on an aluminum supporting platform suspended from a low-friction air bearing system, which allowed precise force measurements. A 2-lbf (8.8964 N) 1D load cell (Futek, model LSB200, item number FSH00092) was used to measure the force along the longitudinal axis.

#### **Experimental procedures**

In the experiments, three independent variables were taken into consideration: ratio between the body height and the height of body plus the fin s/l, the actuation frequency f and incoming flow speed  $U_{\infty}$ . Five experimental sets were performed by changing the body height (s), so that five different s/l ratios could be obtained, as seen in table 1. In each set, the frequency were varied from 1 Hz to 3 Hz in steps of 0.5 Hz, under two flow conditions: without flow, and with a constant incoming flow speed ( $U_{\infty}=11~{\rm cm~s^{-1}}$ ).  $U_{\infty}=11$ cm s<sup>-1</sup> is approximately a swimming speed of 0.4 body length per second (BL/s) that is in the range of swimming speeds of live animals [8, 17] (see table 2). The experimental sets without any body segments (s/l = 0) were conducted first and then body plates of different heights were attached to measure the force at various frequencies under the two flow conditions.

#### Force measurements

The 2-lbf load cell to measure the net surge force of the undulating ribbon fin was connected to amplifier (Futek, model CSG10). One end of the load cell was attached to the downstream side of air-bearing with the robotic model and the other end was fixed to an unmovable structure (mechanical ground). Therefore,

**Table 2.** Kinematics and Reynolds number comparison.  $BL = \text{Body length}, L_{fin} = \text{fin length}, U_{sw} = \text{swimming velocity}$  (for the experimental model  $U_{sw}$  was taken as the incoming flow velocity),  $\lambda = \text{wavelength}, f = \text{fin frequency}, A_{pp} = \text{peak-peak}$  wave amplitude (for A. albifron the value is based on the wave amplitude at the mid-length of the fin),  $V_{wave} = \text{wave velocity}, Re_{\lambda} = \lambda V_{wave}/\nu$ : Reynolds number based on wavelength and wave velocity,  $Re_{\lambda pp} = A_{pp}(fA_{pp})/\nu$ : Reynolds number based on fin height and fin tip velocity and  $St = fA_{pp}/U_{sw}$ . For  $Re_{\lambda pp}$  the low and high limits are based on the limits of the fin frequency, for A.  $Albifrons A_{pp}$  was taken as 1.56 cm. A. Albifrons data is from [17] and A. A. Alvalva data is from [8].

Variable	A. albifron	A. calva	Experimental model
BL, cm	13	30.1	28
$L_{fin}$ , cm	10	13.6	23
$U_{sw}$ , BL s <sup>-1</sup>	0-2.5	0.1-0.8	0.48
$\lambda$ , cm	2.5-4.4	6.41	23
f, Hz	4.5-10	1.8-3.9	1–3
$A_{pp}/\lambda$	0.4-0.5	0.14	0.15
$V_{wave}$ , cm s <sup>-1</sup>	11.3-43.6	12.5-25	23-69
$Re_{\lambda}$ (10 <sup>4</sup> )	0.28-1.92	0.74-1.6	5.3-15.9
$Re_{A_{pp}}$	1095-2409	145-314	1170-3509
$U_{sw}/V_{wave}$	0.5-0.7	0.5-0.9	0.2-0.5
St	0.5-0.7	0.16-0.45	0.3-0.9

the motion of the fin model was restricted by the load cell. Each measurement was taken with a sampling frequency of 1000 Hz and lasted for 10 s after the initial transient period had passed (approximately 30 s). Before each run, the calibration of the load cell was checked and the force measurement of the fin without actuation (0 Hz) were taken. To evaluate the force generation of the fin at different actuation parameters, the mean forces with time were calculated. The force measurement data were filtered using a six-pole Butterworth filter in Matlab with a cutoff frequency of four times the actuation frequency plus 1 Hz to capture other periodic forcing terms.

#### Force analysis

The force measured by the load cell,  $F_{net\ fin}$ , includes both the net force generated by the fin plus the drag of the robotic body. This force can be expressed as,

$$F_{net \ surge} = F_{net \ fin} - D_{body} \tag{1}$$

where  $F_{net\ surge}$  is the net force generated by the undulating fin and  $D_{body}$  is the drag of the body and the fin without actuation (frequency 0 Hz).  $F_{net\ fin}$  includes the thrust generated by the undulating fin and the drag of the fin.  $D_{body}$  was measured for the different body-panels at  $U_{\infty}=11\,\mathrm{cm}\,\mathrm{s}^{-1}$ . Note that for  $U_{\infty}=0\,\mathrm{cm}\,\mathrm{s}^{-1}$ ,  $D_{body}=0$  and  $F_{net\ surge}=F_{net\ fin}$ .

The performance of the fin was evaluated using the mean net force generated by the fin. Although using the thrust generate by the fin would be ideal, decoupling the drag and thrust of the undulating fin is not trivial. Bale *et al* [14] has provided insight in ways to separate drag and thrust. However, drag-thrust decomposition could be prone to errors due to lack of an appropriate

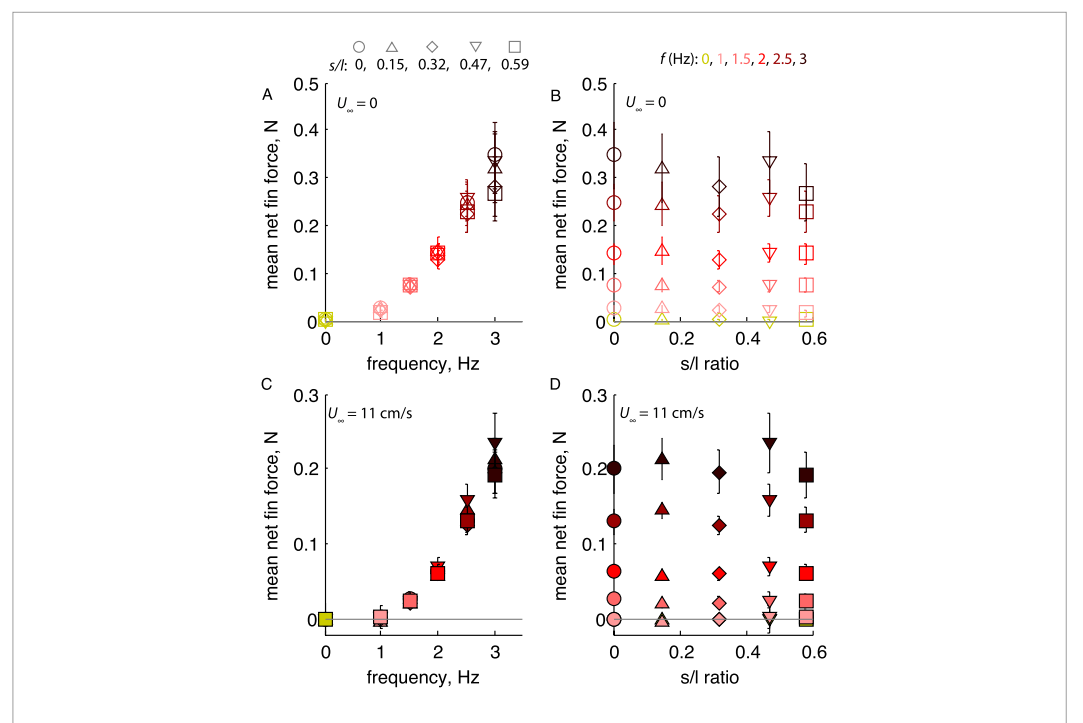


Figure 4. Mean net force generated by the fin as a function of frequency (left) and s/l (right) for  $U_{\infty}=0$  (top) and  $U_{\infty}=11\,\mathrm{cm\,s^{-1}}$  (bottom). Symbols of different shapes represent the results of different s/l, and results of different frequencies are color-coded. Open and filled symbols indicate the results with  $U_{\infty}=0$  and  $U_{\infty}=11\,\mathrm{cm\,s^{-1}}$ , respectively.

drag model to capture the realistic features of the finmembrane.

 $F_{net\ fin_0}$ , the net force generated by the fin without a body attached, was used as a base to compare the net force generated by the fin with different body-heights. The experimental momentum enhancement was defined as  $\beta_F = F_{net\ fin}/F_{net\ fin_0}$ .

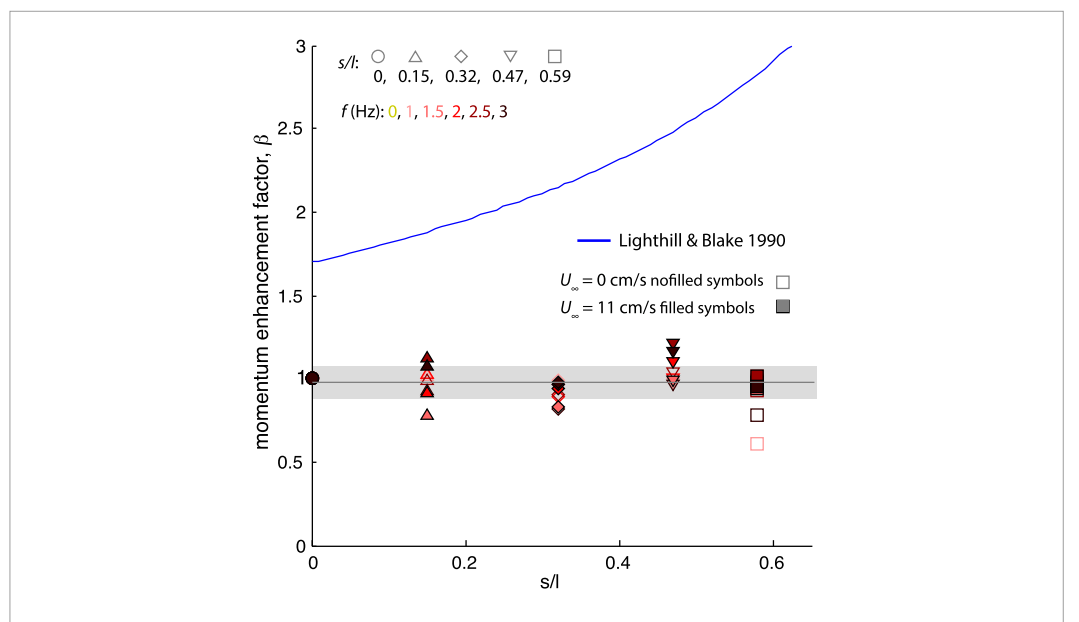
#### **Kinematics**

Table 2 shows a comparison of various kinematics parameters of two fish: A. albifrons (black ghost knifefish) and A. calba (bowfin) and the experimental model parameters. The undulating kinematics of the experimental model were prescribed as sinusoidal traveling wave with a maximum deflection angle of 20 degrees and an oscillation frequency between 1 Hz to 3 Hz. To improve the resolution of the traveling wave in the robotic fin, the wavelength was fixed to one wavelength per fin length. Two Reynolds numbers were defined: (1)  $Re_{\lambda} = \lambda V_{wave}/\nu$ : based on wavelength, wave velocity and the kinematic viscosity of the fluid,  $\nu$ ; and (2)  $Re_{h_{fin}} = h_{fin}(fh_fin)/\nu$ : based on the fin height and tip velocity. Note that since the experimental model was attached to a load cell the freely swimming velocity,  $U_{sw}$ , of the experimental model was not possible to be measured. For the experimental model  $U_{sw}$  was taken as the incoming flow velocity. Even though the frequency range of the robot is in the range (for A. calba ) or below the range (A. albifrons), the Reynolds numbers are higher for the robotic device due to its larger fin height and wavelength. However, the Reynolds number are in the same or similar order of magnitude. Also note that, the frequency of knifefishes has been reported up to 15 Hz [10], resulting in higher Reynolds number. In similar fashion, the Strouhal number considered in the experimental model are in the range of live animals.

## Results and discussion

Five experimental configurations were considered using a robotic ribbon fin model with different body heights as shown in figure 3(A). In each set, the surge force was measured for a varying fin frequency, f, and two flow speeds  $U_{\infty} = [0, 11]$  cm s<sup>-1</sup>. Figure 3(B) shows the net force generated by the fin against time with s/l = 0 and  $U_{\infty} = 0$ . Figure 3(C) shows the corresponding mean net force generated by the fin and the standard deviation of the force. Note that the force measured by the load cell,  $F_{net surge}$ , is a combination of the drag of the body,  $D_{body}$  and the mean net force generated by the fin,  $F_{net\ fin}$ . Thus, the mean net force generated by the fin can be expressed as  $F_{net\ fin} = F_{net\ surge} + D_{body}$ . The net force generated by the fin can be further divided into the thrust and drag of the fin. However, the separability of the thrust and drag of the fin is not straightforward. This issue has been extensively discussed by Bale et al [14].

The mean net fin force is shown as a function of frequency (on the left) and s/l (on the right) in figure 4. The top two panels are for the cases with no incoming flow and the bottom two panels for an incoming flow at  $11 \text{ cm s}^{-1}$ . Different symbols represent different s/l values, and results at different fre-



**Figure 5.** Momentum enhancement as a function of s/l. Solid blue line: analytical momentum enhancement factor proposed by Lighthill and Blake. Symbols: experimental data for different s/l; red-color scale represents frequency, gray solid line: mean momentum enhancement for all the experimental data (0.97); gray area: standard deviation ( $\pm 0.1$ ).

quencies are color-coded. As expected, the mean net fin force increases with frequency for all *s/l* ratios. In addition, the standard deviation increases with frequency. On the right panels, we observe at lower frequencies (2 Hz and under), the fin with different *s/l* values generate almost the same propulsive force. At relatively higher frequencies (2.5 Hz and 3 Hz), the net force generated by the fin at different *s/l* only exhibits small variations.

To consider the effect of body height, a force momentum enhancement factor,  $\beta_F$ , was defined as,

$$\beta_F = \frac{F_{net fin}}{F_{net fin_o}} \tag{2}$$

where  $F_{net\ fin_o}$  is the force generated by the fin without a body attached, and  $F_{net\ fin}$  is the net fin force at different s/l with all the other actuation parameters held constant. This term is equivalent to the momentum enhancement factor presented by [4], and it provides a direct metric to the question posed by Lighthill and Blake, whether an undulating fin is able to generate more propulsive force when a rigid body is above or below the fin.

Figure 5 shows the momentum enhancement factor as a function of s/l measured and the theoretical curved found by Lighthill and Blake [4]. The mean of the measured momentum enhancement factor is 0.97 (shown as a gray solid line) taking into account various s/l ratios, frequencies and the two flow speeds. The gray area represents the standard deviation of  $\pm$  0.1. Therefore, the data show no propulsive momentum enhancement for a fin undulating in presence of a rigid body. This is in agreement with recent numerical

studies of this problem by Bale *et al* [14] and Sprinkle *et al* [15].

The basis of Lighthill and Blake's momentum enhancement factor is due to an increment in the added mass or reactive force experience by the fin as it undulates attached to a rigid body resulting in higher momentum transfer by the fin to the fluid. As the fin is locally twisted along its length, the reactive force experienced by the fin will contribute to a positive propulsive force. This will result in an increase of the mean propulsive force generated by the fin compared to a fin without body.

The calculation for the momentum enhancement developed by Lighthill and Blake was for a 2D flow, considering a cross-section of the body and the fin. As they acknowledge, this scenario is very unrealistic. Furthermore the momentum enhancement for their 2D case would be for the lateral force, making no contribution to the mean propulsive force. However, they argued that in reality the fin is twisted and this local twist in the plane of the fin will make a positive contribution to the propulsive force. Although such propulsive force enhancement due to the fin-body interaction has certain rationality for ribbon-fin-based propulsion, the experimental data show no evidence of such momentum enhancement.

The discrepancy between the Lighthill and Blake's theoretical prediction and the experimental results can be interpreted by noting that the primary mechanism of thrust generated by undulating ribbon fin is a longitudinal jet along the bottom edge of the fin instead of the cross-sectional fluid motion assumed by Lightill and Blake. The streamwise central jet generated by the

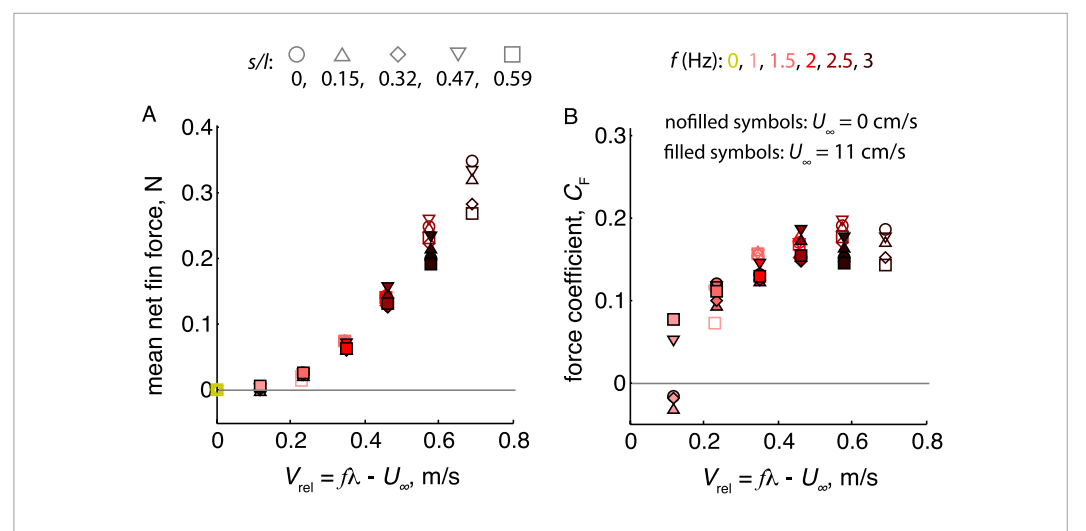


**Figure 6.** Mean net fin force and force coefficient. (A) Mean net fin force as a function of relative velocity,  $V_{rel}$ , between wave speed and incoming flow. (B) Force coefficient,  $C_D$  as a function of relative velocity. Symbols in different shapes represent different s/l values, frequency is represented by colors, no-filled symbols are for  $U_{\infty}=0$  cm s<sup>-1</sup> and filled symbols are for  $U_{\infty}=11$  cm s<sup>-1</sup>.

ribbon fin has been verified by numerical simulations [18] and experimental methods using a robotic device [12, 19, 20]. MacIver *et al* [21] pointed out that the relative size of the body and the ribbon fin is such that it tends to optimize the cost of transport.

The propulsive force generated by the undulating fin can be collapsed to a single curve as function of relative velocity,  $V_{rel}$ , between the traveling wave along the fin  $(V_{wave} = f\lambda)$  and the ambient flow  $(U_{\infty})$ , figure 6(A). The data show a remarkably uniform trend, regardless of the s/l ratio, undulating frequency and incoming flow speed. Similar to previous work on undulating fin propulsion [3, 14, 16], this finding strongly supports the conclusion that the fin force generation depends on the relative motion between the traveling wave along the fin and surrounding fluid.

A coefficient of force for the undulating fin is given by the ratio of the mean net force generated by the fin to the force related to the dynamic pressure as follows:

$$C_F = \frac{F_{net fin}}{0.5\rho S_{enc} V_{rol}^2} \tag{3}$$

where  $\rho$  is the fluid density,  $S_{enc}$  is the enclosed area swept by the tip of the fin and  $V_{rel} = f\lambda - U_{\infty}$  is the relative velocity between the traveling wave and incoming flow. It was found that all the thrust coefficients generally exhibit a uniform varying trend that increase with relative velocity until it peaks around  $V_{rel} = 0.6$  before it starts to decay, figure 6(B). Note that there are three negative data points at 1 Hz with incoming flow. These negative values are most likely because drag of the body and/or drag fo the fin dominates the thrust generation.

Although the results show no evidence of momentum enhancement, it is important to note that similar to Lighhill and Blake, only the fin-body configuration

where the longitudinal axis is parallel to the flow were tested. Many fishes with fin-base propulsion have a relative angle between the longitudinal fin axis and the swimming direction in part to increase propulsive force [19] and/or to improve sensing volume [21]. Future work should address the body-fin interaction at different relative angles with respect to the free-stream velocity.

# **Conclusions**

Gymnotiform, amiiform and balistiform swimmers generate propulsive force by undulating ribbon fins while keeping their bodies almost rigid. The question of whether there is an advantage of the hydrodynamic interaction between the body and the undulating fin was theoretically investigated by Lighthill and Blake [4]. Their findings suggested that the thrust produced by an undulating ribbon fin attached to a rigid body is considerably higher than a single fin itself, which is referred as momentum enhancement. In this work, this momentum enhancement factor was tested for gymnotiform swimmers using a robotic ribbon fin model composed of twelve fin rays interconnected by an elastic membrane with an adjustable body height. In a series of experiments, the surge force generated by the fin was measured as the body height and frequency were changed for two different flow speeds and a constant fin height. The results show that the net force generated by the fin is not strongly affected by the presence of the body attached to it, thus leading to no momentum enhancement. This finding suggests that if there exists an advantage of rigid-body swimming or an evolutionary adaption of the specific body-fin ratio for undulatory-fin-based swimmers, the momentum enhancement due to the interaction between the body and the undulating fin is not the cause.

# Acknowledgments

This material is based upon work supported by the National Science Foundation under Grant No. 1751548 to OMC. We also thank Stewart Glegg for his comments and suggestions.

#### Additional information

#### **Contributions**

IE and OMC designed and performed the experiments; OMC, IE and HL analyzed the data. OMC, IE and HL wrote the paper.

# **Competing interests**

The authors have no competing interests.

#### **ORCID** iDs

Oscar M Curet https://orcid.org/0000-0002-3202-6841

## References

- [1] Korsmeyer K E, Steffensen J F and Herskin J 2002 Energetics of median and paired fin swimming, body and caudal fin swimming, and gait transition in parrotfish (Scarus schlegeli) and triggerfish (Rhinecanthus aculeatus) *J. Exp. Biol.* **205** 1253–63
- [2] Liu H, Gong F and Curet O 2017 Unleashing the potential of undulating fin propulsion using a biomimetic robotic vessel Mar. Technol. Soc. J. 51 79–93
- [3] Curet O M, Patankar N A, Lauder G V and MacIver M A 2011 Mechanical properties of a bio-inspired robotic knifefish with an undulatory propulsor *Bioinspiration Biomimetics* 6 026004
- [4] Lighthill J and Blake R 1990 Biofluiddynamics of balistiform and gymnotiform locomotion. Part 1. Biological background, and analysis by elongated-body theory J. Fluid Mech. 212 183–207
- [5] Lighthill J 1990 Biofluiddynamics of balistiform and gymnotiform locomotion. Part 2. The pressure distribution arising in two-dimensional irrotational flow from a general symmetrical motion of a flexible flat plate normal to itself J. Fluid Mech. 213 1–10

- [6] Lighthill J 1990 Biofluiddynamics of balistiform and gymnotiform locomotion. Part 3. Momentum enhancement in the presence of a body of elliptic cross-section J. Fluid Mech. 213 11–20
- [7] Lighthill J 1990 Biofluiddynamics of balistiform and gymnotiform locomotion. Part 4. Short-wavelength limitations on momentum enhancement J. Fluid Mech. 213 21–8
- [8] Jagnandan K and Sanford C P 2013 Kinematics of ribbon-fin locomotion in the bowfin, amia calva J. Exp. Zool. A 319 569–83
- [9] Near T J et al 2012 Resolution of ray-finned fish phylogeny and timing of diversification Proc. Natl Acad. Sci. 109 13698–703
- [10] Blake R 1983 Swimming in the electric eels and knifefishes Can. J. Zool. 61 1432–41
- [11] Bale R, Neveln I D, Bhalla A P S, MacIver M A and Patankar N A 2015 Convergent evolution of mechanically optimal locomotion in aquatic invertebrates and vertebrates PLoS Biol. 13 e1002123
- [12] Curet O M, Patankar N A, Lauder G V and MacIver M A 2010 Aquatic manoeuvering with counter-propagating waves: a novel locomotive strategy J. R. Soc. Interface 8 1041–50
- [13] Blake R and Chan K 2011 Biomechanics of swimming in the pufferfish diodon holocanthus: propulsive momentum enhancement is an adaptation for thrust production in an undulatory median and paired-fin swimmer *J. Fish Biol.* 79 1774–94
- [14] Bale R, Shirgaonkar A A, Neveln I D, Bhalla A P S, MacIver M A and Patankar N A 2014 Separability of drag and thrust in undulatory animals and machines Sci. Rep. 47329
- [15] Sprinkle B, Bale R, Bhalla A P S, MacIver M A and Patankar N A 2017 Hydrodynamic optimality of balistiform and gymnotiform locomotion Eur. J. Comput. Mech. 26 1–13
- [16] Liu H, Taylor B and Curet O M 2017 Fin ray stiffness and fin morphology control ribbon-fin-based propulsion Soft Robot. 4 103–16
- [17] Ruiz-Torres R, Curet O M, Lauder G V and MacIver M A 2013 Kinematics of the ribbon fin in hovering and swimming of the electric ghost knifefish J. Exp. Biol. 216 823–34
- [18] Shirgaonkar A A, Curet O M, Patankar N A and MacIver M A 2008 The hydrodynamics of ribbon-fin propulsion during impulsive motion J. Exp. Biol. 211 3490–503
- [19] Neveln I D, Bale R, Bhalla A P S, Curet O M, Patankar N A and MacIver M A 2014 Undulating fins produce off-axis thrust and flow structures J. Exp. Biol. 217 201–13
- [20] Liu H and Curet O 2018 Swimming performance of a bio-inspired robotic vessel with undulating fin propulsion *Bioinspiration Biomimetics* 13 056006
- [21] MacIver M A, Patankar N A and Shirgaonkar A A 2010 Energyinformation trade-offs between movement and sensing PLoS Comput. Biol. 6 e1000769